ROYAL SOCIETY OF CHEMISTRY

PAPER

Check for updates

Deep-blue emission and thermally activated delayed fluorescence *via* Dimroth rearrangement of tris(triazolo)triazines†

Ryoga Hojo, [ID] * Don M. Mayder [ID] and Zachary M. Hudson [ID] *

Three luminescent donor–acceptor compounds were prepared based on the Dimroth rearrangement of tris(triazolo)triazines (TTT). In comparison to the non-rearranged TTT isomers, the Dimroth isomer (TTTD) exhibits a substantial blue-shift in emission while maintaining thermally activated delayed fluorescence (TADF) properties. Out of the series of emitters, **TTTD-3HMAT** exhibits deepest blue emission with CIE(x, y) < (0.16, 0.03) and unity quantum yield in toluene, a narrower emission band, and highest two-photon cross-section of 1001 GM owing to the nature of the planarized HMAT donor. **TTTD-3tBu** also exhibits unity quantum yield and deep-blue emission with CIE(x, y) < (0.16, 0.05) in toluene. Finally, **TTTD-3ACR** exhibits TADF with blue-shifted emission and prolonged delayed lifetime due to the slightly larger ΔE_{ST} of 0.26 eV in comparison to the non-rearranged isomer. Overall, this work demonstrates a practical strategy to convert TTT-based donor–acceptor materials to their Dimroth isomers, opening the door to deeper blue-emitting TADF materials with TTT-type acceptors.

Department of Chemistry, The University of British Columbia, 2036 Main Mall, Vancouver, British Columbia, V6T 1Z1, Canada. E-mail: zhudson@chem.ubc.ca; Fax: +1-604-822-2847; Tel: +1-604-822-3266

† Electronic Supplementary Information (ESI) available: A synthetic scheme towards aryl tetrazoles; ^{1}H and ^{13}C{^{1}H} NMR spectra, solvatochromic and AIE properties, nanosecond PL decay curves, cyclic voltammetry data, Tauc plots, time-resolved emission spectra and computational results for **TTTD-3HMAT**, **TTTD-3tBu**, **TTTD-3ACR**. See DOI: https://doi.org/10.1039/d2tc01153k

Dr Zachary M. Hudson is an Associate Professor and Canada Research Chair in Sustainable Chemistry at the University of British Columbia. Zac completed his BSc and PhD in Chemistry at Queen's University, developing luminescent materials for organic electronics. During his PhD he also held graduate fellowships at Jilin University (China) as well as Nagoya University (Japan). He then completed postdoctoral fellowships in polymer science at the University

Zachary M. Hudson

of Bristol (UK) and the University of California, Santa Barbara (USA). He currently leads a research program at UBC developing luminescent materials for optoelectronics, bioimaging, and photocatalysis.

Introduction

Since the seminal work by Adachi and co-workers revealing the phenomenon of thermally activated delayed fluorescence (TADF) in purely organic donor–acceptor materials,[1] substantial progress has been made in realizing their use in the organic light-emitting diode (OLED) display industry.[2–6] TADF materials are of interest as they can harvest energy from both singlet and triplet excitons through reverse intersystem crossing (RISC).[1,3,5,7] Therefore, with TADF materials, 100% internal quantum efficiencies can be achieved in OLED devices without the need for rare-earth metals.[1,8] In recent years, the applications of TADF materials have grown beyond display technology, most notably to encompass time-gated biological imaging[9–14] and organo-photocatalysis.[15–19] To further encourage the mainstream adoption of TADF materials in both biology and chemistry, new donor–acceptor motifs displaying TADF remain critical to furthering emitter design and practical applications.

TADF behaviour is achieved by reducing the energy gap between a molecule's lowest excited singlet and triplet states (ΔE_{ST}), which can be achieved by lowering the electron exchange energy through the spatial separation of the HOMO and LUMO.[1,20] In terms of donor–acceptor design, this process of minimizing ΔE_{ST} can be achieved by inducing a large dihedral angle between the donor–acceptor moieties.[1,21] If ΔE_{ST} is sufficiently small (<0.3 eV), thermal energy enables upconversion from the triplet to singlet excited state, allowing for RISC. Despite this seemingly simple design strategy,

minimizing ΔE_{ST} is often done at the cost of broad and red-shifted emission, due to the strong charge-transfer (CT) character of this donor–acceptor design.[22,23] For this reason, designing efficient deep-blue emitting TADF materials remains one of the biggest challenges in this field.[2,24,25]

In recent years [1,2,4]-triazolo-[1,3,5]-triazine (TTT) has attracted significant attention in the realm of blue-emitting TADF materials due to their weak electron-withdrawing ability.[26–30] The synthesis for this unique heterocyclic motif features cyclization of aryl tetrazoles onto cyanuric chloride under basic conditions.[31,32] To date, several derivatives of TTT-based TADF materials have been successfully synthesized with respectable device performance.[26–30] Our group has also revealed the remarkable two-photon cross-section of TTT-based emitters using hexamethylazatriangulene (HMAT) donors, which has great potential for biological imaging using two-photon excited fluorescence (2PEF).[33]

Following the synthesis of TTT reported in the original paper by Hoffman *et al.*,[34] Tartakovsky and co-workers[31] reported the thermal isomerization process of TTT derivatives, uncovering the Dimroth isomer, TTTD. Similarity in 2018, Detert explored the TTTD isomer in the design of discotic liquid crystals.[35] The Dimroth rearrangement involves thermal ring-transformation of 1,2,3 triazoles,[36,37] whereas for TTT derivatives, the process involves a threefold ring-opening and ring-closing mechanism (Scheme 1).[31,35] More recently, the You group demonstrated a mono-fused (triazolo)triazine derivative undergoing the Dimroth rearrangement to produce efficient TADF emitters with minimal ΔE_{ST} (Scheme S1A, ESI†).[38] Inspired by this work, we hypothesized that the Dimroth rearrangement would provide a unique opportunity to observe the effect of thermal isomerization on TTT compounds; and precisely observe the change in TADF behavior.

Herein we report the synthesis of three compounds, **TTTD-3HMAT**, **TTTD-3tBu**, and **TTTD-3ACR**, based on the Dimroth rearrangement of donor-acceptor materials bearing a TTT core. **TTTD-3HMAT** and **TTTD-3tBu** exhibit unity photoluminescence quantum yields (PLQYs) in both solution and the solid-state, with **TTTD-3HMAT** exhibiting deeper-blue emission and a higher two-photon cross-section (σ^2) in toluene relative to **TTTD-3tBu**. Finally, **TTTD-3ACR** retains TADF character with blue-shifted emission compared to the non-rearranged TTT

emitter. Indeed, **TTTD-3ACR** represents the deepest blue emitter displaying TADF behaviour to date based on the TTT acceptor motif.

Results and discussion

The pre-rearranged TTT compounds were synthesized according to previous reports, involving reaction of donor-functionalized tetrazoles with cyanuric chloride (Scheme S1B, ESI†).[33] The procedure for the Dimroth rearrangement was adapted from the procedure of You and coworkers (Scheme S1A, ESI†),[38] by heating the TTT compounds to 200 °C under basic and inert conditions. Reaction times varied from 3–7 days, as monitored by thin layer chromatography (Scheme 2). Specifically, the thermal conversion to synthesize **TTTD-3tBu** and **TTTD-3ACR** was completed after three days, while synthesis of **TTTD-3HMAT** required seven days to achieve full conversion. The characteristic downfield shift in the donor aryl-hydrogen signals at ∼8 ppm in the ^{1}H NMR spectra relative to the starting material TTT isomer, and the retained symmetry in both ^{1}H and ^{13}C{^{1}H} NMR spectra (Fig. S1–S7, ESI†) agree with previous reports suggesting a symmetric Dimroth-rearranged tris(triazolo)triazine.[35]

Our method contrasts with the synthetic route reported by You and co-workers involving a Pd-catalyzed cross-coupling on the pre-assembled and Dimroth-rearranged (triazolo)triazine (Scheme S1A, ESI†). Our results demonstrate that thermal rearrangement can reliably occur after the donors are appended to the acceptor, providing a direct synthetic route without the use of palladium. Moreover, we also attempted a Pd-catalyzed coupling using a triiodide-functionalized Dimroth-rearranged TTT acceptor, for cross-coupling with amine-based donors; the insolubility of tris(*p*-iodophenyl)-TTTD made this method unfeasible and challenging to characterize (Scheme S1C, ESI†). We also attempted to synthesize and characterize TTTD derivatives bearing 10*H*-phenoxazine (**TTTD-3POX**) or 10*H*-phenothiazine donors (**TTTD-3PTZ**) by thermal rearrangement. In these cases, however, the products were highly insoluble in common organic solvents, likely due to extensive π-stacking (Scheme S1C, ESI†). No glass transitions could be observed for the three isolated compounds between 30–200 °C by differential scanning calorimetry (Fig. S16, ESI†).

The UV-visible absorption and photoluminescence (PL) spectra of TTTD emitters in toluene are given in Fig. 1A. The absorption maxima ranged from 298 nm to 391 nm, with **TTTD-3HMAT** and **TTTD-3tBu** exhibiting small Stokes shifts of 25 nm and 58 nm, respectively (Table 1). PLQYs of 1.0 were observed for both **TTTD-3HMAT** and **TTTD-3tBu**, while **TTTD-3HMAT** exhibited deeper blue emission (416 nm) and smaller FWHM (42 nm) in toluene, attributed to the restricted intermolecular motion of the planarized donors. In contrast, a weak charge-transfer absorption band is observed for **TTTD-3ACR**, with a broader emission profile and an emission maximum at 461 nm in toluene. In addition, an increase in PLQY from 0.26 under air to 0.41 in N_2-sparged solution is observed for **TTTD-3ACR** in
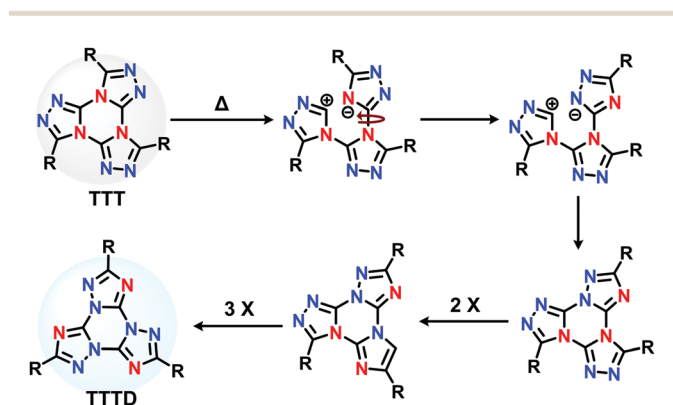
Scheme 1 The isomerization of TTT to TTTD.[35]
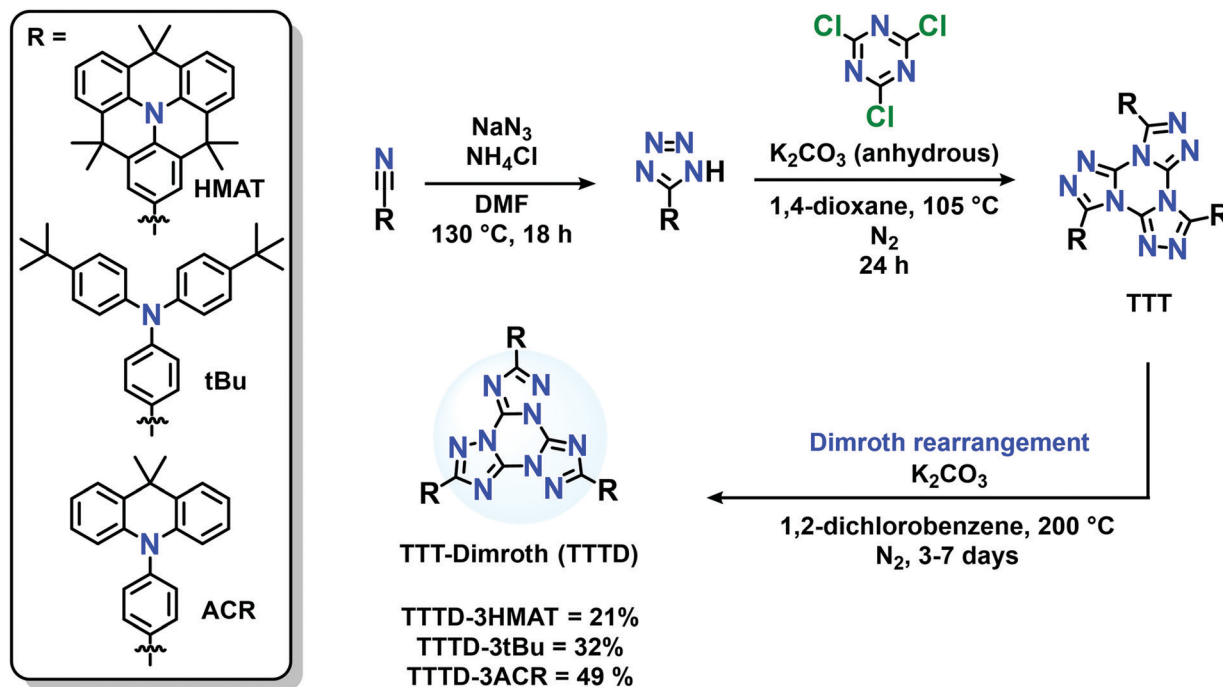
Scheme 2 Synthetic route to donor–acceptor Dimroth-rearranged TTTD compounds.

Fig. 1 (A) Solution-state absorption (dashed) and fluorescent emission under air (solid) measured in toluene at optical densities of 0.05 (λ_{exc} = 350 nm). (B) Two-photon absorption of TTTD emitters (C) CIE diagram showing the chromaticity of the emitters in toluene measured under air.

toluene, suggesting the likely involvement of triplet states in the emission mechanism. The prompt fluorescence PL decays in toluene (Fig. S7A, ESI†) were also measured using time-correlated single-photon counting (TCSPC): the lifetime for **TTTD-3HMAT** and **TTTD-3tBu** ranged from 2.1 to 2.6 ns, while the lifetime for **TTTD-3ACR** is slightly longer at 7.6 ns (Table 1).

Multi-channel scaling (MCS) was then used to analyze the longer-lived PL decays in solution (Fig. S8A, ESI†). While **TTTD-3HMAT** and **TTTD-3tBu** show no observable delayed lifetime in both ambient and inert conditions, **TTTD-3ACR** exhibits a delayed lifetime of 19 μs in oxygen-free conditions, likely arising from delayed fluorescence.

This journal is © The Royal Society of Chemistry 2022

J. Mater. Chem. C, 2022, **10**, 13871–13877 | **13873**

Table 1 Summarized solution and solid-state absorption, emission, and lifetime data

Entry	Solution						3 wt% in PMMA			
	$\lambda_{abs}{}^{a}$ (nm) ε (10^4 cm^{-1} M^{-1})	$\lambda_{em/FWHM}{}^{a}$ (nm)	$\sigma_{740}{}^2$ (GM)	$\Phi_{air}/\Phi_{N_2}{}^{b/c}$	$\tau^{air\,a}$	$\tau^{N_2\,c}$	$\lambda_{em/FWHM}{}^{d}$ (nm)	$\Phi_{air}{}^{d}$	$\tau^{air\,d}$	$\tau^{vac\,e}$
TTTD-3HMAT	298 (11), 391 (11)	416/42	1001	1.00/1.00	2.1 ns	2.3 ns	425/56	1.00	2.7 ns	2.7 ns
TTTD-3tBu	298 (4.1), 370 (10)	428/58	845	1.00/1.00	2.6 ns	2.6 ns	432/60	1.00	3.5 ns	3.5 ns
TTTD-3ACR	363 (0.5)	461/74	83	0.26/0.41	7.6 ns	11 ns/19 μs	453/130	0.14	9.2 ns/107 μs^f	9.2 ns/13 ms^f

[a] Measured in toluene under air at 0.01 mg mL^{-1}. [b] Absolute photoluminescence quantum yields determined using an integrating sphere. [c] Measured in toluene solutions sparged with N$_2$. [d] Measured under air at 298 K. [e] Measured under vacuum at 298 K. [f] Amplitude-weighted lifetime measurement *via* multiexponential tail fitting.

Aggregation-induced emission (AIE) and solvatochromism experiments were conducted to investigate the nature of the CT properties of these three materials. AIE experiments were conducted using water/THF mixtures, with water fractions (f_w) ranging from 0% to 99%. The emission intensity increased as the percentage of water increased for **TTTD-3ACR**, with an overall 170% enhancement at f_w = 70% Fig. S9, ESI†. In contrast, **TTTD-3HMAT** and **TTT-3tBu** lack AIE character. A positive solvatochromic shift is observed for all emitters, from least to most polar solvents (Fig. S10, ESI†). However, a minimal solvatochromic shift is observed with **TTTD-3HMAT** and **TTT-3tBu**. In contrast, the significant solvatochromic shift observed for **TTTD-3ACR** is evidence of strong CT character, consistent with its TADF behaviour (Fig. S10, ESI†).[21,39,40]

The two-photon cross-sections (σ^2) for TTTD compounds were examined over the range of 710–850 nm using 2PEF measurements (Fig. 1B). Using (*E*)-4,4′-(ethene-1,2-diyl)-bis(*N,N*-diphenylaniline) in dichloromethane as a blue-emitting reference dye standard, all measurements were periodically checked to verify a square dependence of signal intensity with excitation power. The highest σ^2 was observed with **TTTD-3HMAT** ($\sigma_{740}{}^2$ = 1001 GM), followed by **TTTD-3tBu** ($\sigma_{740}{}^2$ = 845 GM) and **TTTD-3ACR** ($\sigma_{740}{}^2$ = 83 GM). In agreement with previous reports, the structural constraints and planar nature of HMAT donors allow for superior two-photon cross-sections, where a high σ^2 value are enhanced with higher planarity and symmetry of the molecule (Table 1).[33,41–43]

Photophysical properties of the emitters in the solid-state were analyzed by preparing poly(methyl methacrylate) (PMMA) films doped with 3 wt% of emitter. Blue-shifted emission is observed with **TTTD-3ACR** (453 nm) relative to the emission maximum in toluene (461 nm). Red-shifted emission is observed with **TTTD-3HMAT** and **TTTD-3tBu**, which can arise from aggregation due to greater π-stacking in these less-twisted materials.[26] Moreover, PLQY values of unity were observed for **TTTD-3HMAT** and **TTTD-3tBu** in the solid state, while that of **TTTD-3ACR** reached 0.14. Under vacuum, the emission intensity of **TTTD-3ACR** rises 2.0-fold compared to an air atmosphere, while intensities for **TTTD-3HMAT** and **TTTD-3tBu** remain essentially unchanged (Fig. S13, ESI†).

PL decays were measured for PMMA-doped films using TSCPC to measure prompt fluorescence (Fig. S1B, ESI†), and MCS was used to analyze the longer-lived PL decays (Fig. S2B, ESI†). Lifetimes of **TTTD-3HMAT** and **TTTD-3tBu** were

consistent under air or vacuum at 298 K, only exhibiting prompt fluorescence in each case. In contrast, **TTTD-3ACR** has a long-lived PL lifetime of 107 μs in air, further lengthened to 13 ms under vacuum (Table 1). To elucidate if the long-lived emission of **TTTD-3ACR** was due to TADF, temperature-dependent lifetime measurements were conducted in the range of 77 to 298 K. As predicted, suppression of delayed fluorescence was observed upon cooling from 298 K to 77 K (Fig. 2). However, the emergence of long-lived phosphorescence is also observed below 200 K, which can be attributed to the restriction of roto-vibrational motion and dominance of phosphorescence emission when reaching cryogenic temperatures. Time-gated and steady-state emission measurements at 77 K of **TTTD-3ACR** in 2-methyltetrahydrofuran further support TADF, with a measured value for ΔE_{ST} of 0.26 eV (Fig. S14, ESI†). Conversely, the larger values of ΔE_{ST} measured for **TTTD-3HMAT** (0.51 eV) and **TTTD-3tBu** (0.35 eV) likely preclude RISC.

The determination of E_{HOMO} and E_{LUMO} were identified using cyclic voltammetry (CV) and Tauc plots (Fig. S11, ESI†). For all emitters, quasi-reversible one-electron oxidation is observed, which is attributed to each donor moiety. An irreversible reduction event is shown for TTTD acceptors within the solvent window of *o*-difluorobenzene. Therefore, Tauc plots were necessary to obtain optical gaps (E_{gap}) from UV-Vis absorption measurements, where the E_{LUMO} ranged from −1.85 eV to −1.92 eV. The trend for E_{gap} is in slight disagreement with the calculated values using DFT (Fig. S12, ESI†). Nevertheless, all emitters display a large E_{gap} around 3.1 eV, expected for deep-blue emitting chromophores (Table 2). Finally, we provide a comprehensive comparison of the

Fig. 2 (A) PL decays for 3 wt% doped PMMA films under air (black) *vs.* vacuum (colored) of **TTTD-3ACR**. (B) PL decays for **TTTD-3ACR** (3 wt% doped PMMA film) at various temperatures between 77–298 K. λ_{ex} = 350 nm.

13874 | *J. Mater. Chem. C*, 2022, **10**, 13871–13877

This journal is © The Royal Society of Chemistry 2022

Table 2 Theoretical and experimental electronic properties

Entry	HOMO/LUMO[ab] (eV)	$E_{gap}^{DFT\,c}$ (eV)	$E_{gap}^{opt\,d}$ (eV)	ΔE_{ST} (eV) Calc.[c]	ΔE_{ST} (eV) Exp.[e]
TTTD-3HMAT	−4.97/−1.91	3.42	3.06	0.38	0.51
TTTD-3tBu	−5.01/−1.85	3.03	3.16	0.46	0.35
TTTD-3ACR	−4.98/−1.92	3.01	3.06	0.006	0.26

[a] HOMO = $-(E_{1/2}^{ox} + 4.8$ eV). [b] LUMO = (E_{gap}^{opt} + HOMO). [c] Theoretical calculations from TDA-DFT at the B3LYP/6-31g(d) level. [d] Calculated using a Tauc plot of the UV-Vis spectrum in toluene. [e] Determined from onsets of time-gated phosphorescence and fluorescence spectra measured in 2-MeTHF at 77 K.

photophysical and electrochemical properties of these TTTD compounds and their TTT isomers in Table S8 (ESI†).

Density functional theory (DFT) at the B3LYP/6-31g+(d) level was used further to analyze the photophysical and electronic properties of the emitters (Fig. 3). Structural optimization was performed at the B3LYP/6-31g+(d) level, followed by the use of the Tamm–Dancoff approximation (TDA) for time-dependent calculations at the B3LYP/6-31g(d) level. TDA-DFT was selected for theoretical calculations, as it has been shown to be suitable for larger molecules that suffer from the triplet instability problem.[44] While diffuse orbitals were used during structural optimization at the B3LYP/6-31g+(d) level, they were not included for TDA-DFT due to the higher computational demand for the large molecules presented here.

In general, theoretical calculations yielded trends in agreement with experimental observations. The calculated ΔE_{ST} for

TTTD-3ACR is the smallest at 0.006 eV, while both **TTTD-3HMAT** and **TTTD-3tBu** have larger calculated ΔE_{ST} values above 0.38 eV. Molecular orbital visualization through natural transition orbitals (NTOs) indicates poor spatial separation of frontier molecular orbitals of the donor and acceptor in **TTTD-3HMAT** and **TTTD-3tBu**. Consequently, the higher calculated oscillator strengths for the S_0 to S_1 transition support the stronger observed CT absorption, and subsequently the high PLQY for these materials as well (Table S1, ESI†). In contrast, the near-orthogonal predicted dihedral angle between the ACR donor and TTTD acceptor in **TTTD-3ACR** induces strong spatial separation between the highest-occupied NTO (HONTO) and lowest-unoccupied NTO (LUNTO). This likely explains the TADF behaviour of **TTTD-3ACR**, yet also limits strong absorption from S_0 to S_1 as indicated by the low oscillator strength of this transition (Fig. 3 and Table S1, ESI†).

Interestingly, a general comparison between TTTD and TTT isomers indicates that each isomer is of similar total energy, with a minimal predicted change in the energy of the S_1 state between each isomer pair (Fig. S15 and Table S1, ESI†). In all three cases, the predicted energies of the S_1 states of the TTT isomers were within 50 meV of the TTTD isomers, when simulated in toluene using a polarized continuum model (PCM).

Conclusion

Here, we have employed the Dimroth rearrangement for a series of donor–acceptor compounds containing the TTT acceptor, revealing the photophysical properties of the TTTD isomer. All three emitters, **TTTD-3HMAT**, **TTTD-3tBu**, and **TTTD-3ACR**, exhibit a deeper blue emission than the TTT isomer. **TTTD-3HMAT** and **TTTD-3tBu** exhibit deep blue emission at λ_{max} = 416 nm and 428 nm, respectively in toluene, while **TTTD-3HMAT** displays a narrow FWHM (42 nm) and high 2PA (σ_{740}^2 = 1001 GM) owing to the nature of the planarized donor groups (Table 1). In contrast, **TTTD-3ACR** retains its TADF character while exhibiting a deeper blue emission (454 nm) in comparison to its TTT isomer. Overall, this work demonstrates the effect of the Dimroth rearrangement on the photophysical and electronic properties of TTT-based donor–acceptor materials. In doing so, we have provided the path toward deeper blue materials based on the TTT framework. Finally, these novel TTTD-based materials may find their use in diverse applications for deep-blue emitters, with potential as high energy sensitizers in photocatalysis, two-photon bioimaging dyes, or as emitters in OLEDs.

Experimental details

General considerations

All reagents were purchased from Oakwood Chemical, Sigma-Aldrich, or Alfa Aesar and used without purification. **HMAT** was synthesized according to previously reported procedures (Scheme S1, ESI†).[45] All yields correspond to the isolated yield.
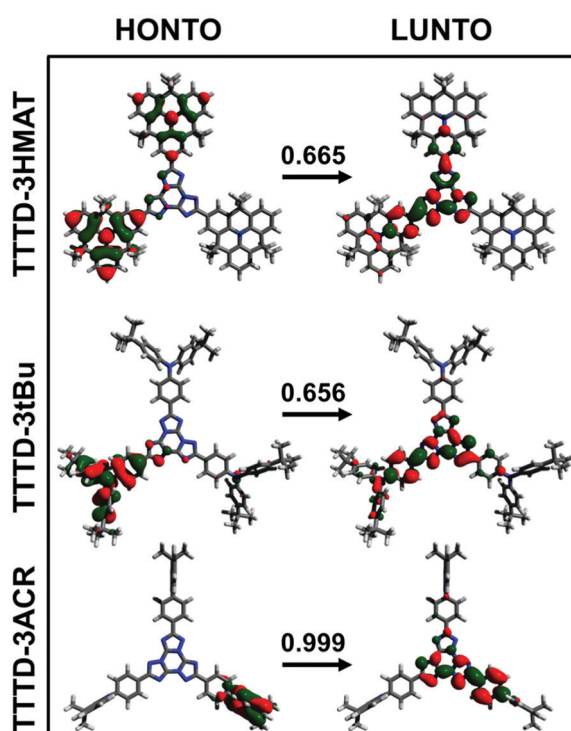

Fig. 3 Pictorial representation of optimized S_0 geometries for TTTD emitters. The weight of the transition between HONTO and LUNTO is indicated above the arrow.

Paper

The ^{1}H and ^{13}C{^{1}H} nuclear magnetic resonance (NMR) spectra were measured on a Bruker Advance 300 Spectrometer or Bruker AV III HD 400 MHz spectrometer with methylene chloride-d_2 (CD$_2$Cl$_2$) or chloroform-d (CDCl$_3$) as the solvent. High resolution mass spectra (HRMS) were obtained with atmospheric pressure chemical ionization (ACPI) or field desorption (FC) using a Waters/Micromass LCT spectrometer. Absorbance measurements were taken using a Cary 60 spectrometer, while fluorescence measurements were obtained from Edinburgh Instruments FS5 spectrofluorometer and Edinburgh Instruments FLS1000 spectrofluorometer was specifically used for time-gated emission measurements. Absolute photoluminescence quantum yields were determined using an Edinburgh Instruments SC-30 Integrating Sphere Module, and samples were prepared at concentrations with optical densities of 0.10 at the excitation wavelength.

Electrochemical methods

Cyclic voltammograms were measured using a BASi Epsilon Eclipse potentiostat at room temperature using a three-electrode configuration (working electrode: 3 mm diameter glassy carbon; reference electrode: RE-5B Ag/AgCl electrode in saturated aqueous KCl (BASi Inc.), referenced externally to ferrocene/ferrocenium; counter electrode: Pt wire) in 0.2 M tetrabutylammonium hexafluorophosphate in o-difluorobenzene. Experiments were conducted at a scan rate of 20 mV s^{-1} in N$_2$-sparged electrolyte solution with 2 mg mL^{-1} of the analyte.

Density functional theory

Quantum chemical calculations were conducted using the Gaussian 16 Rev. B.01 package with default settings unless otherwise stated. Ground state energies and corresponding geometries were calculated at the B3LYP/6-31g+(d) level of theory. Tamm–Dancoff approximation (TDA)-DFT was performed from the optimized frequencies at the B3LYP/6-31g(d) level of theory. Molecular orbitals were visualized using Avogadro version 1.20 and rendered using POV-Ray version 3.7.0.

General procedure for the Dimroth rearrangement from TTT to TTTD

The Dimroth rearrangements of tris(triazolo)triazines were conducted according to a modified literature procedure.[38] To a 100 mL Schlenk flask equipped with a magnetic stir bar was added tris(triazolo)triazines (0.493 mmol, 1 equiv.), K$_2$CO$_3$ (1.97 mmol, 4 equiv.), and anhydrous 1,2-dichlorobenzene (50 mL). The reaction mixture was sparged with N$_2$ for 15 min before being heated to 200 °C for 3–7 days (3 days for **TTTD-3tBu** and **TTTD-3ACR**, 7 days for **TTTD-3HMAT**) using a preheated oil bath under N$_2$ atmosphere. Upon completion, the reaction was cooled to room temperature. Once cooled, the crude reaction was filtered to remove K$_2$CO$_3$, and the filtrate was concentrated *in vacuo*. The crude residue was purified by column chromatography over silica gel to yield the pure tris(triazolo)triazine compound.

TTTD-3HMAT. Purified over silica (1 : 1 hexanes : EtOAc) resulting in yellow solid. Yield: 21 mg (21%). ^{1}H NMR (300 MHz, CD$_2$Cl$_2$) δ 8.42 (s, 6H), 7.51–7.45 (m, 12H), 7.20 (dd, J = 7.6 Hz, 6H), 1.79 (s, 36H), 1.68 (s, 18H) ppm. ^{13}C{^{1}H} NMR (101 MHz, CD$_2$Cl$_2$): ^{13}C NMR (101 MHz, CD$_2$Cl$_2$) δ 165.1, 144.7, 135.1, 131.3, 130.4, 130.3, 130.1, 124.0, 123.6, 123.5, 122.8, 122.5, 35.7, 35.4, 33.4, 32.7 ppm. HRMS (APCI) m/z: [M]$^+$ calc'd for [C$_{87}$H$_{78}$N$_{12}$]$^+$ 1290.6466; found 1290.6472; 0.49 difference ppm.

TTTD-3tBu. Purified over silica (3 : 2 hexanes : EtOAc) resulting in yellow solid. Yield: 198 mg (32%). ^{1}H NMR (300 MHz, CD$_2$Cl$_2$) δ 8.14 (ddd, J = 8.2 Hz, 6H), 7.38–7.35 (m, 12H), 7.14–7.11 (m, 12H), 7.07 (ddd, J = 8.8 Hz, 6H) 1.34 (s, 54H) ppm. ^{13}C{^{1}H} NMR (101 MHz, CD$_2$Cl$_2$): ^{13}C NMR (101 MHz, CDCl$_3$) δ 165.1, 151.1, 147.1, 144.4, 144.1, 128.8, 126.3, 125.3, 120.2, 119.8, 34.4, 31.5 ppm. HRMS (APCI) m/z: [M]$^+$ calc'd for [C$_{83}$H$_{87}$N$_{12}$]$^+$ 1266.7399; found 1266.7411; difference 0.99 ppm.

TTTD-3ACR. Purified over silica (1 : 1 hexanes : CHCl$_3$) resulting in yellow solid. Yield: 295 mg (49%). ^{1}H NMR (300 MHz, CDCl$_3$) δ 8.74 (ddd, J = 8.4 Hz, 6H), 7.59 (ddd, J = 8.4 Hz, 6H), 7.49 (ddd, J = 5.9 Hz, 6H), 7.04–6.93 (m, 12H), 6.38 (ddd, J = 6.5 Hz, 6H), 1.72 (s, 18H) ppm. ^{13}C{^{1}H} NMR (101 MHz, CDCl$_3$): δ 164.8, 144.8, 144.7, 140.5, 132.0, 130.5, 130.4, 127.8, 126.4, 125.4, 121.0, 114.1, 36.1, 31.2 ppm. HRMS (FD) m/z: [M]$^+$ calc'd for [C$_{69}$H$_{54}$N$_{12}$]$^+$ 1050.4536; found 1050.4545; difference 0.92 ppm.

Conflicts of interest

There are no conflicts to declare.

Acknowledgements

References

1 H. Uoyama, K. Goushi, K. Shizu, H. Nomura and C. Adachi, *Nature*, 2012, **492**, 234–238.

2 A. Monkman, *ACS Appl. Mater. Interfaces*, DOI: **10.1021/acsami.1c09189**.

3 X. Cai and S. J. Su, *Adv. Funct. Mater.*, 2018, **28**, 1–33.

4 Z. Yang, Z. Mao, Z. Xie, Y. Zhang, S. Liu, J. Zhao, J. Xu, Z. Chi and M. P. Aldred, *Chem. Soc. Rev.*, 2017, **46**, 915–1016.

5 H. Lim, H. J. Cheon, S. J. Woo, S. K. Kwon, Y. H. Kim and J. J. Kim, *Adv. Mater.*, 2020, **32**, 1–8.

6 Y. Tang, Y. Liu, W. Ning, L. Zhan, J. Ding, M. Yu, H. Liu, Y. Gao, G. Xie and C. Yang, *J. Mater. Chem. C*, 2022, **10**, 4637–4645.

7 D. Hu, L. Yao, B. Yang and Y. Ma, *Philos. Trans. R. Soc., A*, 2015, **373**, 20140318.

8 Y. C. Duan, L. L. Wen, Y. Gao, Y. Wu, L. Zhao, Y. Geng, G. G. Shan, M. Zhang and Z. M. Su, *J. Phys. Chem. C*, 2018, **122**, 23091–23101.

9 N. R. Paisley, S. V. Halldorson, M. V. Tran, R. Gupta, S. Kamal, W. R. Algar and Z. M. Hudson, *Angew. Chem., Int. Ed.*, 2021, **60**, 18630–18638.

10 C. J. Christopherson, N. R. Paisley, Z. Xiao, W. R. Algar and Z. M. Hudson, *J. Am. Chem. Soc.*, 2021, **143**, 13342–13349.

11 A. M. Polgar and Z. M. Hudson, *Chem. Commun.*, 2021, **57**, 10675–10688.

12 Q. Zhang, S. Xu, M. Li, Y. Wang, N. Zhang, Y. Guan, M. Chen, C. F. Chen and H. Y. Hu, *Chem. Commun.*, 2019, **55**, 5639–5642.

13 V. N. Nguyen, A. Kumar, M. H. Lee and J. Yoon, *Coord. Chem. Rev.*, 2020, **425**, 213545.

14 S. Qi, S. Kim, V. N. Nguyen, Y. Kim, G. Niu, G. Kim, S. J. Kim, S. Park and J. Yoon, *ACS Appl. Mater. Interfaces*, 2020, **12**, 51293–51301.

15 E. R. Sauvé, C. M. Tonge and Z. M. Hudson, *J. Mater. Chem. C*, 2021, **9**, 4164–4172.

16 M. A. Bryden and E. Zysman-Colman, *Chem. Soc. Rev.*, 2021, **50**, 7587–7680.

17 Z. Mao, A. Huang, L. Ma and M. Zhang, *RSC Adv.*, 2021, **11**, 38235–38238.

18 C.-L. Dong, L.-Q. Huang, Z. Guan, C.-S. Huang and Y.-H. He, *Adv. Synth. Catal.*, 2021, **363**, 3803–3811.

19 D.-F. Chen, C. H. Chrisman and G. M. Miyake, *ACS Catal.*, 2020, **10**, 2609–2614.

20 C. M. Marian, *Annu. Rev. Phys. Chem.*, 2020, **72**, 617–640.

21 S. Weissenseel, N. A. Drigo, L. G. Kudriashova, M. Schmid, T. Morgenstern, K. H. Lin, A. Prlj, C. Corminboeuf, A. Sperlich, W. Brütting, M. K. Nazeeruddin and V. Dyakonov, *J. Phys. Chem. C*, 2019, **123**, 27778–27784.

22 X. Yang, X. Xu and G. Zhou, *J. Mater. Chem. C*, 2015, **3**, 913–944.

23 R. Huang, N. A. Kukhta, J. S. Ward, A. Danos, A. S. Batsanov, M. R. Bryce and F. B. Dias, *J. Mater. Chem. C*, 2019, **7**, 13224–13234.

24 D. Zhang and L. Duan, *Nat. Photonics*, 2021, **15**, 173–174.

25 J. H. Lee, C. H. Chen, P. H. Lee, H. Y. Lin, M. K. Leung, T. L. Chiu and C. F. Lin, *J. Mater. Chem. C*, 2019, **7**, 5874–5888.

26 S. K. Pathak, Y. Xiang, M. Huang, T. Huang, X. Cao, H. Liu, G. Xie and C. Yang, *RSC Adv.*, 2020, **10**, 15523–15529.

27 F. Hundemer, E. Crovini, Y. Wada, H. Kaji, S. Bräse and E. Zysman-Colman, *Mater. Adv.*, 2020, **1**, 2862–2871.

28 S. Wang, X. Wang, K. H. Lee, S. Liu, J. Y. Lee, W. Zhu and Y. Wang, *Dyes Pigm.*, 2020, **182**, 108589.

29 Z. Fang, S. Wang, J. Liao, X. Chen, Y. Zhu, W. Zhu and Y. Wang, *J. Mater. Chem. C*, 2022, 38–43.

30 S. Zeng, C. Xiao, J. Zhou, Q. Dong, Q. Li, J. Lim, H. Ma, J. Y. Lee, W. Zhu and Y. Wang, *Adv. Funct. Mater.*, 2022, 2113183.

31 V. A. Tartakovsky, A. E. Frumkin, A. M. Churakov and Y. A. Strelenko, *Russ. Chem. Bull.*, 2005, **54**, 719–725.

32 S. Glang, T. Rieth, D. Borchmann, I. Fortunati, R. Signorini and H. Detert, *Eur. J. Org. Chem.*, 2014, 3116–3126.

33 R. Hojo, D. M. Mayder and Z. M. Hudson, *J. Mater. Chem. C*, 2021, **9**, 14342–14350.

34 O. E.-K. A. Hofmann, *Ber. Dtsch. Chem. Ges.*, 1911, **44**, 2713–2717.

35 H. Detert, *Eur. J. Org. Chem.*, 2018, 4501–4507.

36 C. Wentrup, M. S. Mirzaei, D. Kvaskoff and A. A. Taherpour, *J. Org. Chem.*, 2021, **86**, 8286–8294.

37 A. Champiré, C. Vala, A. Laabid, A. Benharref, M. Marchivie, K. Plé and S. Routier, *J. Org. Chem.*, 2016, **81**, 12506–12513.

38 R. Su, Y. Zhao, F. Yang, L. Duan, J. Lan, Z. Bin and J. You, *Sci. Bull.*, 2021, **66**, 441–448.

39 R. Ansari, W. Shao, S.-J. Yoon, J. Kim and J. Kieffer, *ACS Appl. Mater. Interfaces*, 2021, **13**, 28529–28537.

40 M. Wang, H. S. Shin, F. Zhou, H. Xu, P. Prabhakaran, B. Dryzhakov, H. Su, K. S. Lee and B. Hu, *J. Phys. Chem. C*, 2020, **124**, 14832–14837.

41 D. M. Mayder, C. M. Tonge, G. D. Nguyen, R. Hojo, N. R. Paisley, J. Yu, G. Tom, S. A. Burke and Z. M. Hudson, *Chem. Mater.*, 2022, **34**(6), 2624–2635.

42 M. Hirai, N. Tanaka, M. Sakai and S. Yamaguchi, *Chem. Rev.*, 2019, **119**, 8291–8331.

43 Z. Fang, T. L. Teo, L. Cai, Y. H. Lal, A. Samoc and M. Samoc, *Org. Lett.*, 2009, **11**, 1–4.

44 F. J.-A. Ferrer, J. Cerezo, E. Stendardo, R. Improta and F. Santoro, *J. Chem. Theory Comput.*, 2013, **9**, 2072–2082.

45 X. K. Chen, Y. Tsuchiya, Y. Ishikawa, C. Zhong, C. Adachi and J. L. Brédas, *Adv. Mater.*, 2017, **29**, 1–8.

This journal is © The Royal Society of Chemistry 2022

J. Mater. Chem. C, 2022, **10**, 13871–13877 | **13877**